Plasma-Chemical and Photo-Catalytic Degradation of Methyl Orange

4 authors, including:

Baghdad Benstaali
Oman Medical College
13 PUBLICATIONS   629 CITATIONS

SEE PROFILE

Nader Al-Bastaki
The Kingdom University
37 PUBLICATIONS   646 CITATIONS

SEE PROFILE

Ahmed Addou
Université Abdelhamid Ibn Badis Mostaganem
106 PUBLICATIONS   1,416 CITATIONS

SEE PROFILE

Some of the authors of this publication are also working on these related projects:

Effect of atmospheric conditions on GRP View project

urinary lithiasis View project

Plasma-chemical and photo-catalytic degradation of methyl orange

Baghdad Benstaali* and Nader Al-Bastaki

Chemical Engineering Department,
University of Bahrain,
Isa Town, P.O. 32038, Bahrain
Fax: +973 17680935
E-mail: bbenstaali@eng.uob.bh
E-mail: benstaal@yahoo.co.uk
E-mail: naderbsk@eng.uob.bh
*Corresponding author

Ahmed Addou

Laboratoire STEVA,
Universite de Mostaganem,
Mostaganem 27000, Algeria
E-mail: addou_ahmed@yahoo.fr

Jean Louis Brisset

Laboratoire LEICA,
UFR des Sciences de l'Universite de Rouen,
76821 Mont Saint-Aignan, France
E-mail: Jean-Louis.Brisset@univ-rouen.fr

Abstract: Non-thermal atmospheric humid air plasma is used to investigate chemical reactions mechanisms of predominantly produced neutral hydroxyl radicals by gliding arc discharges with Methyl Orange (MO). UV/Visible spectroscopy and electrochemical measurements were performed. Treated solutions show that highly reactive $HO^\bullet$ radicals interaction favours the creation of intermediate species followed by their degradation leading to one aromatic ring end product. Photocatalytic (UV/TiO_2 and UV/H_2O_2) treatments lead to the complete decolourisation of MO within few minutes. The results obtained may confirm that the final product of air plasma MO interaction contains NO_2 and NH_2 groups, the consequence of $^\bullet NO$ presence in plasma.

Keywords: non-thermal plasma; advanced oxidation process; MO; methyl orange; titanium dioxide; hydrogen peroxide.

Biographical notes: Baghdad Benstaali is an Associate Professor in the Chemical Engineering Department at the University of Bahrain. He earns

a PhD in Physics and a Doctorat d'Etat in Chemistry. Using emission spectroscopy, he identified and quantified neutral radicals species produced in humid air plasma. He actually teaches analytical measurement courses and introduced gliding discharges for the treatment of liquid industrial wastes for environmental applications. He co-authored several papers in the area of non-thermal plasma applications.

Nader Al-Bastaki is currently the Dean of the College of Engineering at the University of Bahrain. Previously, he was the Chair of the Chemical Engineering Department and the Director of the Accreditation and Assessment Office. His recent research areas include treatment of coloured waste water using nanofiltartion membranes, combined ultrafiltration and adsorption and UV/TiO$_2$ photocatalytic oxidation.

Ahmed Addou is the Director of the Laboratory of Sciences and Techniques of Environment and Valorization (STEVA) at the University of Mostaganem. He prepared his thesis in chemistry at the University of Lille, France. His main research interests are environmental and supervised several research projects using gliding arc discharges for the degradation of industrial wastes. He is co-author of numerous papers, and books.

Jean-Louis Brisset prepared his Thesis in Paris-VI University. He was appointed Professor at Rouen University (1990) and responsible for the Laboratory of Electrochemistry and Analytical Chemistry. He retired in 2006 and was nominated Emeritus Professor. He developed electrical gliding discharges for liquids treatment and focused on the chemical properties of activated species formed in the plasma gas. He brought special attention to the forthcoming applications of electrical discharge to the degradation of organic wastes in liquid effluents, and inactivation of bacteria. He is co-author of numerous papers, patents and books. He often referees manuscripts for highly specialised journals.

1 Introduction

There is an increasing interest in reducing the significant toxic effect of azoic dyes on the environment due to their wide utilisation in various industrial processes and manufacturing industries, and a large number of papers are thus devoted to the destruction of these dyes. Therefore understanding the oxidation mechanisms of azoic dyes becomes necessary and diverse means of oxidation processes: peracids (Oakes and Gratton, 1998), photocatalytic degradation (Rashed and El-Amin, 2007; Li et al., 2007; Mozia et al., 2005; Yu et al., 2005), photocatalytic with oxygen micro bubbles (Tasaki et al., 2008), photocatalytic oxidation with titanium dioxide (Guetta and Ait Amar, 2005) advanced oxidation process (Heba et al., 2008), contact glow discharge electrolysis (Gong et al., 2008; Gong and Cai, 2007; Gao, 2006), pulsed corona discharge (Grabowski et al., 2007), gliding electrical discharge (Brisset et al., 2008; Moussa et al., 2007; Abdelmalek et al., 2004), have been used. Azoic dyes are characterised by an azo bond connected to aromatic rings or heterocycles. Various substitutes can be found such as alkyl, amino, hydroxy, halogeno, sulphonate or more complex groups. While dyes containing azo or hydrazo link are more resistant to peracid oxidation, they are completely discoloured using photocatalytic oxidation. The present study deals with

di-methyl-amino-azo-benzene sulfonic acid commonly called Methyl Orange (MO) which is among the most widely used dyes and well known as a coloured indicator. The investigation focuses on the interaction of neutral radicals species produced by non thermal discharge (or 'glidarc') plasma of humid air and their chemical effect on MO with and without the presence of equal concentration of titanium dioxide (TiO_2) as a catalyst.

Spectral investigation of the gliding arc discharge in humid air showed the occurrence of two major species, the predominant $HO^\bullet$ and $^\bullet NO$ (Benstaali et al., 1999, 2002). These species were identified from their emission bands and their population was quantified. $^\bullet NO$ was characterised by the $^\bullet NO$ ($a^2\Sigma^+ - X^2\Pi$, $\Delta v = -1, -2, -3$) γ system at 237 nm and the $HO^\bullet$ by the $HO^\bullet$ ($a^2\Sigma^+ - X^2\Pi$, $\Delta v = 0$) system at 306 nm. $HO^\bullet$ and $^\bullet NO$ present interesting chemical properties: $HO^\bullet$ is a strong oxidising species, ranking just after fluorine with a standard potential $E°(HO^\bullet/H_2O) = 2.85$ V/SHE. $HO^\bullet$ is also able to form dimers H_2O_2 in the plasma treated solution, and this secondary species (Brisset et al., 2008) is also known as a strong oxidising agent. $^\bullet NO$ is the precursor of a set of reactions which leads to the formation of transient nitrous acid and nitric acid in the target solution (Brisset et al., 2008). The change of unstable nitrous to stable nitric acid involves a transient intermediate, peroxynitrous acid, which also presents strong oxidising properties $E°(HOONO/N_2O) = 2.85$ V/SHE. The resulting acid effect enhances the oxidising power of the impinging species as often observed when organic compounds are concerned with oxidation reactions.

In photocatalytic treatments, TiO_2 catalyst suspensions in aqueous solutions are exposed to UV radiations to produce $HO^\bullet$ radicals which should oxidise dissolved organic materials responsible for coloured solutions. Since the atmospheric plasma produced $HO^\bullet$ and $^\bullet NO$ radicals are identified through their UV emission spectra (Benstaali et al., 2002), the presence of UV photosensitive catalyst such as TiO_2 may enhance the treatment. UV radiations interact with TiO_2 to produce additional $HO^\bullet$ radicals in the solution. The purpose of this investigation was to make a comparative analysis between atmospheric non thermal plasma of humid air and UV photocatalytic interaction with MO. The oxidation procedure and the reaction kinetics were separately monitored by UV/Vis molecular absorbance spectroscopy, pH and conductivity measurements.

2   Experimental section

2.1   The plasma source

A detailed description of the experimental device that was largely developed by Czernichowski and co-workers for industrial applications (Fillon et al., 1990; Lesueur et al., 1988; Jorgensen et al., 1987) is illustrated in Figure 1.

Pressurised air led through a bubbling distilled water flask gets water saturated before entering the glidarc reactor through a nozzle of diameter ϕ. It goes through two semi elliptic electrodes supplied with a 220 V/10 kV high voltage Aupem Sefli transformer that produces an alternative potential difference of constant amplitude V. The mean operating parameters are 160 mA and 600 V in working conditions. The electric charges $+Q$ and $-Q$ produced at the electrodes surface gather at the elliptic small curvature region. The electric arc generated between the electrodes when varying the electrodes

shape, is pushed down the increasing electrodes gap e at a gas flow speed before breaking at the arc length threshold. The gas flow rate Q_v, which can be expressed in L.min^{-1}, is measured by a Show Rate Brooks flow metre.

Figure 1   Experimental set-up of an atmospheric gliding arc reactor
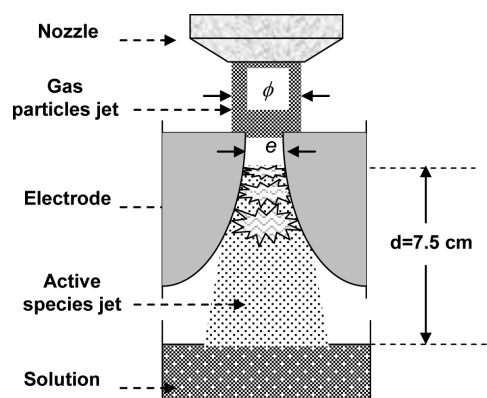
2.2   UV radiations source

The UV radiation source is a UVP grid design mineralight lamp model R-52 which produces a highly uniform 254 nm UV radiation of high intensity of 1250 µW/cm at 15.24 cm with the filter. It is generated by 230 V 50/60 Hz and produces 0.45 Ampere. The distance between the UV lamp to the liquid solution surface is kept constant at 3 cm. Once exposed to UV radiations of 254 nm for a period of treatment, the magnetically stirred MO sample solution is taken away from the UV source while keeping the UV light source on.

2.3   Solution preparation and treatment conditions

The Methyl Orange dye (formula $C_{14} H_{14} N_3 O_3 S Na$; molar mass 327.3 g), also referred to as Orange III, 4′-Dimethylaminoazobenzene-4-sulfonic acid, sodium salt or more commonly named Heliantine, was purchased from Aldrich and used to prepare a stock solution of known concentration (10^{-2} mol L^{-1}) by dissolving the powder in distilled water. Methyl Orange is an acid-base indicator (pK_a: 3.5) with absorption peaks at 464 nm and 507.5 nm for the yellow-orange basic and red acid forms respectively. The initial solution 10^{-2} mol L^{-1} is red and turns to orange when diluted to a concentration of 7.8×10^{-5} mol L^{-1}. Another mixture of equal concentration of 7.8×10^{-5} mol L^{-1} of MO and titanium (IV) oxide (TiO$_2$) of molecular weight 79.90 g mol^{-1} supplied by Sigma-Aldrich was prepared. A magnetically stirred 80 mL volume of the mixture was placed at a distance of $d = 7.5$ cm from the ignition point of the electrical arc and treated by a non thermal plasma of humid air at a flow rate $Q = 10$ L min^{-1}. Each treatment period of $T = 30$ s was followed by measurements of absorbance, pH and electrolytic conductivity. A double beam UV-Vis Schimadzu spectrometer 1601 model with 900 lines/mm holographic grating was used to follow the absorbance of plasma treated solutions. pH measurement were made using a Metrohm pH metre model 780.

Electrolytic conductivity measurements were obtained using an EC 215 Hanna Instruments conductivity metre using a thermostated cell.

3   Results and discussions

3.1   UV-visible spectrometry results

3.1.1   Plasma treatment of MO

The UV/Vis absorbance spectra of MO treated by humid air plasma are shown in Figures 2 and 3. The initial MO solution of concentration of 7.8 x 10^{-5} mol L^{-1} (pH = 6) shows a broad absorption peak at the wavelength 464.5 nm with an absorbance value 1.83 (molar absorption coefficient $\varepsilon_{4645nm} = 2.34 \times 10^4$ L mol^{-1} cm^{-1}) and a shoulder at a lower wavelength 415 nm. The molecular coefficient at the shoulder is calculated $\varepsilon_{415\,nm} = 1.64 \times 10^4$ L mol^{-1} cm^{-1}. The maximum absorption peak at 465 nm was already observed at different conditions (40°C and pH = 9.6) in previous literature (Oakes and Gratton, 1998) and at 464 nm (Magureanu et al., 2007). At pH = 6.3, MO shows an absorption peak at 463 nm with $\varepsilon_{463nm} = 2.356 \times cm^{-1}$ imputed to transition of azo group while a slight shoulder appears around 400 nm attributed to the transition of the same azo group (Thomas and Burgess, 2007).

Figure 2   UV/Visible spectra of MO treated by humid air plasma for 0–2.5 min
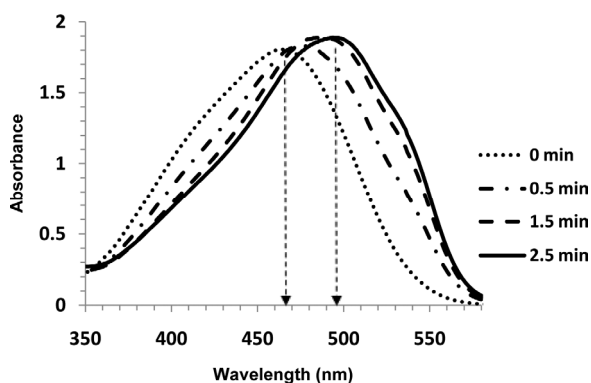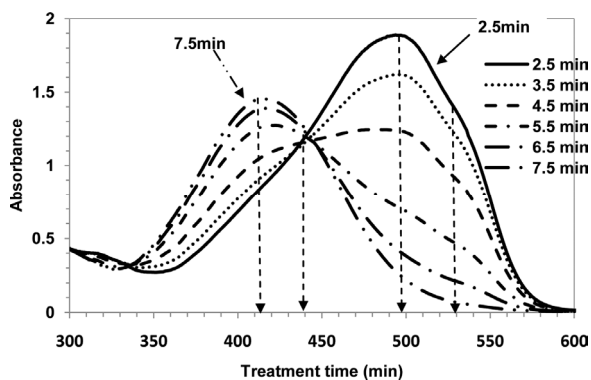

Figure 3   UV/Visible spectra of MO treated by plasma for 2.5–7.5 min

When exposed during fixed periods of 30 s to the plasma of humid air, the treated MO solution shows a shift of the absorption band initially centred at $\lambda_{max} = 464.5$ nm to higher wavelength and higher absorbance of the absorption peak with treatment time. The absorbance at the shoulder 415 nm on the other hand decreases with time. Longer exposure to the plasma of humid air shows variation of the absorption band with the treatment time which suggests that the treated MO solution is undergoing a set of complex reactions involving acid transform and oxidation processes as a result of chemical reactions with non thermal plasma produced neutral reactive species HO$^\bullet$. The presence of less dominant neutral radicals $^\bullet$NO creates acidic medium encouraging chemical reactions to take place. Previous investigations of reactions mechanisms taking place in plasma produced by contact glow discharge electrolysis proposed that produced species in the discharge gap are accelerated due to a steep potential gradient and enter the air-liquid interface with an energy that may be greater than 100 eV (Gong et al., 2008; Sengupta et al., 1998).

Therefore energy transferred from excited radicals HO$^\bullet$ and $^\bullet$NO to MO molecules in the solution may be high enough to provoke a cleavage of the azo groups causing fragmentation of MO molecules into smaller groups. Dye oxidation is accompanied by the reduction of oxygen to hydrogen peroxide where the first stage of oxidation involves demethylation of MO followed by cleavage of the azo bond to give colourless products (Darwent and Lepre, 1986). Decomposed fragments may combine with oxided MO molecules to form other molecules that absorb at different wavelengths. Following the first 30 s of exposure to the reactive species, MO absorption band initially centred at $\lambda = 464.5$ nm shows a shift towards the red, in agreement with the acid evolution of the solution. Within two and a half minutes of treatment time, the shifting absorption peak stabilises at 495 nm with a second shoulder appearing at higher wavelength 536.5 nm. The one minute treatment visible spectrum shows a maximum of absorption at 481 nm with the two shoulders appearing on both sides 415 nm and 536.5 nm (Figure 2). Within the time interval [0–2.5 min] of treatment time, spectra show a more pronounced second shoulder at 536.5 nm emerging whilst the first one at 415 nm disappearing (Figures 2 and 3). The absorbance values at different wavelengths corresponding to the maximum absorption peaks that are 464.5 nm, 495 nm, and 415 nm are presented in Figure 4. The absorbance values at the 464.5 nm and 495 nm maximum absorption peaks are 1.8062 and 1.9137, respectively.
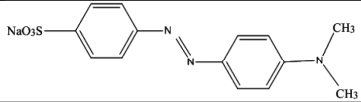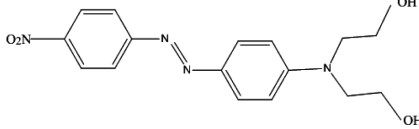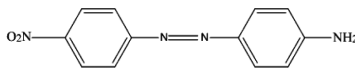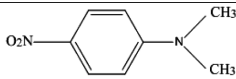
Figure 4   Absorbance variation at 464.5 nm, 495 nm and 415 nm of MO
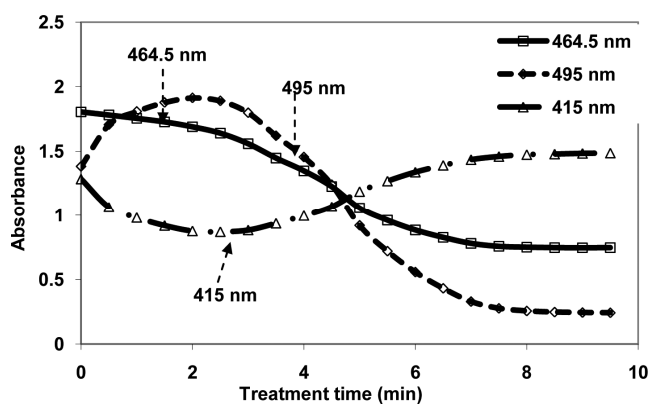
As a result of increasing released protons H^+, $^\bullet NO$ species and their derivatives in the solution, the pH decreases and MO undergoes colour changes from the initial yellow-orange (pH = 6) to more pronounced orange (pH = 3.7–3.3) and back to lesser orange for more acid media (pH < 3.2). This may suggest that the azo bond linking the two aromatic rings is preserved. Modification of its structure by exchanging substituents leads to other types of MO. The decrease of the absorbance of MO at 464.5 nm accompanied by a shift in the absorption band at higher wavelength 495 nm and colour changes may suggest that some molecules at the interface of the plasma liquid solution are degraded into small fragments that recombine with oxided non-degraded molecules to form another type of dyes. It is therefore clear that the structure of MO has been changed and the maximum peak shifts from 464.5 nm to 495 nm after plasma treatment of MO solution, while the absorbance values at these peaks are more or less equal, indicates that the MO in the presence of plasma produced reactive species is undergoing Direct Chemical Oxidation (DCO) by oxidising hydroxyl radicals $HO^\bullet$. Similar phenomenon is explained by the degradation of MO in the presence of peroxydisulphate ions (Zhong et al., 2008). Potassium peroxydisulfate (KPS) can be effective in hazardous wastewaters in acidic or basic media through DCO (McCallum et al., 2000).
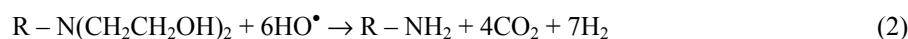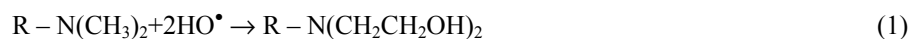
First suggestions may be that MO tends to become Disperse Red 19 (DR19) ($C_{16}H_{18}N_4O_4$) that absorbs at 495 nm (Sigma Aldrich) and Methyl Red (MR) ($C_{15}H_{15}N_3O_2$) at 540 nm (Lacheb at al., 2002). Reactive Red 141 dye concentration was determined by monitoring the absorbance at 530 nm (Telke et al., 2008). The evolution of the maximum absorption peak of the solution suggests that MO is undergoing various chemical reaction mechanisms (ionisation, excitation, cleavage, and recombination) that are explained in Table 1.

Table 1　　Chemical reaction mechanisms of reactive species with MO

Product	Molecular Structure	Chemical reactions
Primary species	$HO^\bullet$, $^\bullet NO$, H, O_x, N_y	Ionization, Excitation Decomposition, Attachment Recombination
Secondary species	H_xO_y, NO_x, HNO, HOONO, HNO_3	
Methyl Orange $C_{14}H_{14}N_3NaO_3S$ $\lambda_{max} = 464.5$nm		Cleavage Ionization, Ion exchange, Oxidation, Recombination
Disperse Red 19 $C_{16}H_{18}N_4O_4$ $\lambda_{max} = 495$nm		
Disperse Orange 3 $C_{12}H_{10}N_4O_2$ $\lambda_{max} = 415$nm		Ionization, Ion exchange, Recombination
(N,N)-dimethyl-4-nitro aniline $\lambda_{max} = 420$ nm		

The chemical reactions mechanisms that are likely to occur and lead to the end products are of:

Oxidative type on the dimethyl group side:

$$R - N(CH_3)_2 + 2HO^\bullet \rightarrow R - N(CH_2CH_2OH)_2 \tag{1}$$

$$R - N(CH_2CH_2OH)_2 + 6HO^\bullet \rightarrow R - NH_2 + 4CO_2 + 7H_2 \tag{2}$$

Acidic type on the sulfonic acid group side:

$$R - SO_3Na_2 + e^- \rightarrow R - (SO_3Na)^- \tag{3}$$

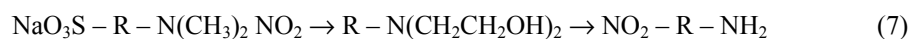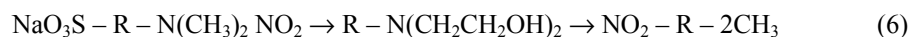$$R - (SO_3Na_2)^- + NO_2 \rightarrow R - NO_2 + (SO_3Na)^- \tag{4}$$
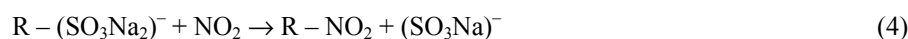
From $t > 7$ min, the solution turns to and stays yellow. The absorbance variation within the time range [8–9.5 min] shows a linear increase at a very small rate of 8.1×10^{-3}. The evolution of the absorbance with the treatment time t^* suggests an overall zero order reaction.

Continuous exposure from 10 to 15 min to the discharge did not have any effect on the solution colour which may lead to suggest that a final product is obtained.

Further treatment leads to a product whose absorbance increases at 415 nm. In presence of increasing number of protons in an acidic medium, methyl groups tend to decompose leading to the formation of amino functional groups NH_2. These results agree with previously reported observation and may be interpreted as the occurrence of an acid base equilibrium between the two matching forms of the indicator and the beginning of the degradation process as described in Moussa et al. (2007) and may be illustrated, according to changes occurring in absorbance spectra (Figure 4), by a set of simultaneous reactions:

$$H_2O + e^- \rightarrow H^\bullet + {}^\bullet OH \, (+e^-) \tag{5}$$

and (2). The occurrence and properties of the discharge products are considered where the final product proposed is an acidic form of the dye N,N-dimethyl-4-nitroaniline through oxidative cleavage of the diazoïc bond (Moussa et al., 2007; Brisset et al., 2008) and confirmed by equation (4). Another type of dye Disperse Orange 3 (DO3) ($C_{12}H_{10}N_4O_2$) is reported to absorb at 415 where the visible portion of the spectrum of Disperse Orange 3 showed a major peak at 415 nm (Hardin et al., 2003). But Aldrich catalogue reports DO3 absorption peak at 443 nm (Aldrich Catalogue, xxx, pp.6, 17). DO3 contains two substituted aromatic rings, one with an amino substituent and the other with a nitro substituent, typical of many monoazo disperse dyes. That type of structure suggests that equations (2) and (4) have taken place leading to DO3. If this case is taking place, we can propose the following chemical reaction mechanism:

$$NaO_3S - R - N(CH_3)_2 \, NO_2 \rightarrow R - N(CH_2CH_2OH)_2 \rightarrow NO_2 - R - 2CH_3 \tag{6}$$

$$NaO_3S - R - N(CH_3)_2 \, NO_2 \rightarrow R - N(CH_2CH_2OH)_2 \rightarrow NO_2 - R - NH_2 \tag{7}$$

3.1.2 *Influence of TiO$_2$ on MO plasma treatment*

The influence of TiO$_2$ catalyst on the plasma treatment of MO was investigated. The pH of the solution was initially at 5.95. In photocatalytic treatments, TiO$_2$ suspensions in aqueous solutions are exposed to UV radiations to produce $HO^\bullet$ radicals which should oxidise dissolved organic materials responsible for colouring solutions. Incidentally, it is worthy to notice that Ti (IV) moieties form a coloured 1 : 1 complex with H_2O_2

(peak wavelength at 410 nm) which is well known for analytical purposes but with a structure still under discussion. Since the atmospheric plasma produced HO$^{\bullet}$ and $^{\bullet}$NO radicals are identified through their UV emission spectra (Benstaali et al., 2002), the presence of UV photosensitive catalyst such as TiO$_2$ may enhance the plasma treatment. UV radiations interact with TiO$_2$ to produce additional HO$^{\bullet}$ radicals in the solution such shown in equations (8) and (9).

$$TiO_2 + h\nu - e^- + h^+ \tag{8}$$

$$H_2O_2 + h^+ \rightarrow HO^{\bullet} + H^+ \tag{9}$$

The other reactions (1)–(4) will follow. Figure 5 shows the variation of the absorbance at different absorption peaks (464.5 nm and 415 nm) of both MO treated by humid air plasma in presence and without TiO$_2$.

Figure 5   Absorbance variation at 464.5 nm and 415 nm for MO and MO + TiO$_2$
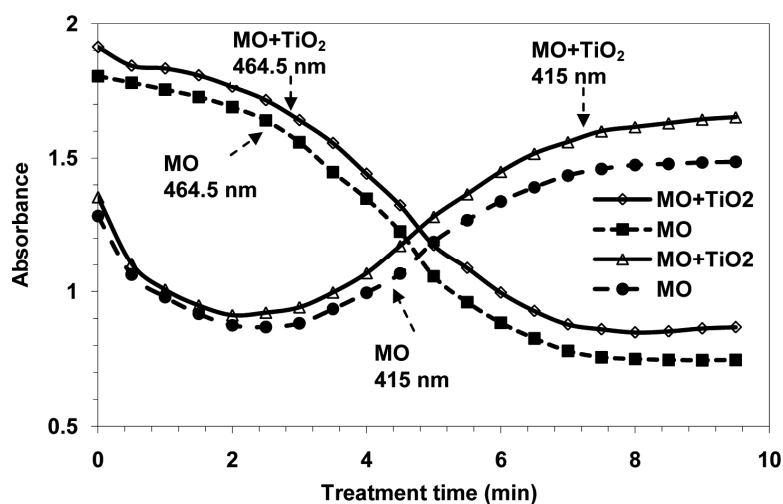
Although the behaviour of MO in presence of TiO$_2$ is similar to the previous one obtained with the appearance and disappearance of intermediate products at the same absorption peaks, the absorbance intensity is somewhat higher (1.92) than that (1.80) obtained without the catalyst. Also the maximum absorption peak does not change; the absorbance of MO + TiO$_2$ solution raises the absorbance to 4.5% more than that of MO alone. The increase of the absorbance is observed during the whole plasma treatment. The presence of the catalyst TiO$_2$ enhances the presence of hydroxyl radicals by producing more through equations (8) and (9) on top of those generated by the plasma. The medium becomes more populated with hydroxyl radicals and the oxidation of MO is more effective. Therefore an increase in DCO is taking place and the absorbance of MO in presence of TiO$_2$ catalyst could be related to an oxidation effect induced by TiO$_2$ on MO. The rates of variation of absorbance have close values whether TiO$_2$ is used or not. The rates of variation of the different maximum absorption peaks of the MO solution with and without catalyst are given in Table 2.

Table 2 Rate of variation of the absorbance at different absorption peaks

	464.5 nm	495 nm	415 nm
MO	-0.0615 (R^2=0.9961) [0 – 2 min]	-0.3989 (R^2=0.9871) [2.5 – 6.5 min]	0.0089 (R^2=0.9595) [8 – 9.5 min]
MO + TiO$_2$	-0.0627 (R^2=0.9353) [0 – 2 min]	-0.4138 (R^2=0.989) [2.5 – 6.5]	0.0292 (R^2=0.9997) [7.5 – 9 min]
MO+H$_2$O$_2$	-0.1452 (R^2=0.9374) [0.5 – 2 min]	-0.8786 (R^2=0.9949) [2.5 – 4 min]	0.0463 (R^2=0.9838) [3 - 4 min]

As we can observe, the rates of variation of the absorption peaks without catalysts are identical within 1% error for the 464.5 and 495 nm absorption peaks. For the 415 nm absorption, the rate of variation is more significant in presence of TiO$_2$. The final product obtained is stable within several days after treatment. The addition of few drops of H$_2$O$_2$ to the final product and its exposure to UV radiations make it loose its yellow colour within 5 min of treatment.

3.1.3 Influence of H$_2$O$_2$ on MO plasma treatment

MO solutions containing H$_2$O$_2$ ($C_{H2O2} = 1.14 \times 10^{-2}$ mol L^{-1}) was also exposed to plasma species. The absorbance spectra are shown in Figure 6. Similar behaviour of spectra to those of MO alone is observed. The absorbance of MO + H$_2$O$_2$ solution at 464.5 nm is slightly higher (2.17) compared to (1.92) of MO + TiO$_2$ and (1.80) of MO alone. It seems that the presence of H$_2$O$_2$ accelerates the speed of direct chemical reactions occurring in the plasma treated MO solution. It reduces the treatment time to reach the maximum absorption peak at 495 nm. One and half minutes are needed for MO + H$_2$O$_2$ to reach the first maximum at 495 nm while it takes 2 min for MO and MO + TiO$_2$.

Figure 6 Absorbance variation of MO + H$_2$O$_2$ at different treatment times
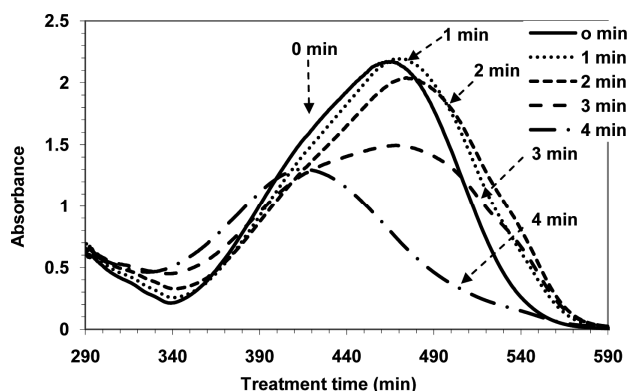
The appearance of the maximum at the same time for MO and MO + TiO$_2$ may be due to the fact that measurements are taken every half minute hiding real maximum. Reducing the period of treatment might reveal the difference between them. This effect is largely observed for the maximum absorption peak at 415 nm for MO + H$_2$O$_2$ and MO where 4 min of plasma treatment for MO + H$_2$O$_2$ solution to reach the appearance of supposed final product (Figure 7) while nine and half minutes treatment time were not enough for MO and MO + TiO$_2$.

Figure 7   Absorbance variation at different peaks for MO + H$_2$O$_2$
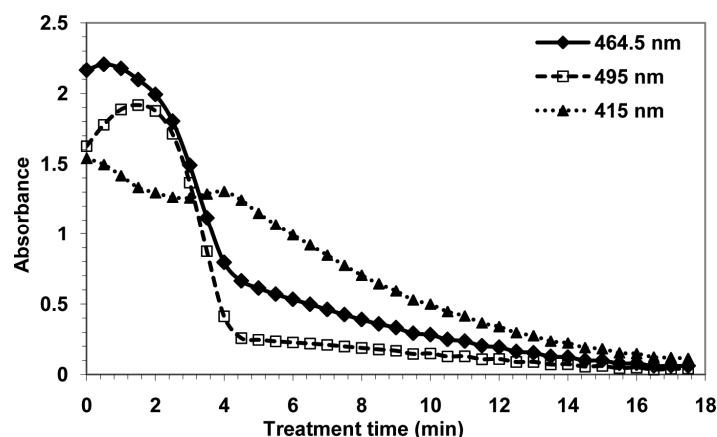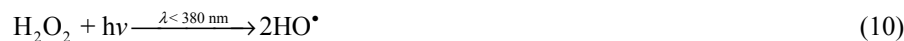

Over 4 min of exposure to the humid air plasma, the absorbance spectra show a decrease of the absorbance at 415 nm followed with a shift of the absorption peak at 390 nm in the UV band (Figure 8). Therefore adding H$_2$O$_2$ to the MO solution reduces the treatment time to nearly 50% of that of MO alone. The reason for such a rapid acceleration effect is due to the production of HO$^\bullet$ radicals through the interaction of UV radiations emitted by NO$^\bullet$ (237 nm) and HO$^\bullet$ (306 nm) radicals with H$_2$O$_2$. These two values are far below the wavelength value 380 nm that initiates the decomposition of H$_2$O$_2$.

Figure 8   Absorbance variation at 415 nm for plasma treated MO + H$_2$O$_2$
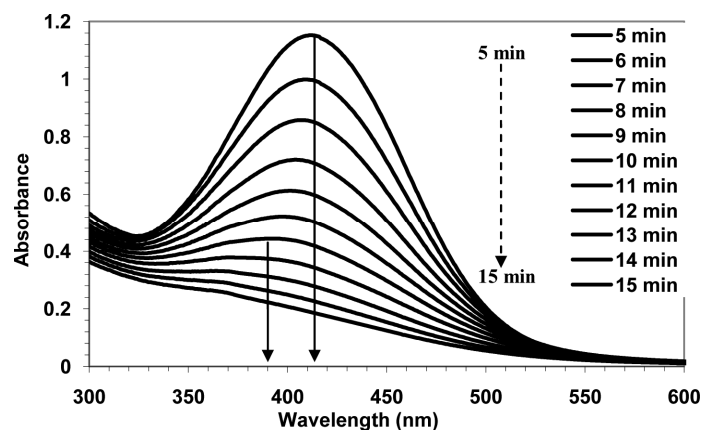
Emitted UV radiations with energies 5.23 eV ($NO^{\bullet}$) and 4.05 eV ($HO^{\bullet}$) are higher than the threshold value 3.26 eV corresponding to the degradation of H_2O_2 into $HO^{\bullet}$ radicals by UV radiations as expressed by equations (10), (11) and (12) (Zhong et al., 2008):

$$H_2O_2 + h\nu \xrightarrow{\lambda < 380\,nm} 2HO^{\bullet} \tag{10}$$

$$^{\bullet}OH + H_2O_2 \rightarrow H_2O + HO^{\bullet}_2 \tag{11}$$

$$HO^{\bullet}_2 + H_2O_2 \rightarrow H_2O + O_2 + {}^{\bullet}OH \tag{12}$$

Other reactions (1)–(4) follow. The exposure of MO solutions to UV radiations alone shows a very low rate of degradation of MO molecules (34% within four hours). The presence of H_2O_2 contributes to the amount of $HO^{\bullet}$ radicals (Haque and Muneer, 2007) and enhances the decomposition rate of MO molecules. Therefore under plasma treatment, we see two simultaneous phenomena of $HO^{\bullet}$ radicals' production: the first one through the electrical discharge interactions with humid air molecules in the plasma gaseous phase while the second one occurs in the aqueous medium through the degradation of H_2O_2 molecules by UV plasma produced radicals themselves.

3.1.4 UV treatment of MO in presence of TiO₂ and H₂O₂

A solution of equal concentration (7.8×10^{-5} mol.L^{-1}) of MO and TiO_2 was prepared with distilled water. 10 ml of MO solution containing TiO_2 and two drops of H_2O_2 (0.05 mL) was exposed at a distance of 3 cm from UV radiations source. Readings were taken every minute for the MO + TiO_2 + H_2O_2 solution. Figure 9 shows the absorbance variation of the solution versus UV exposure time.

Figure 9 Absorbance variation of MO+TiO2+H2O2 under UV radiations exposure
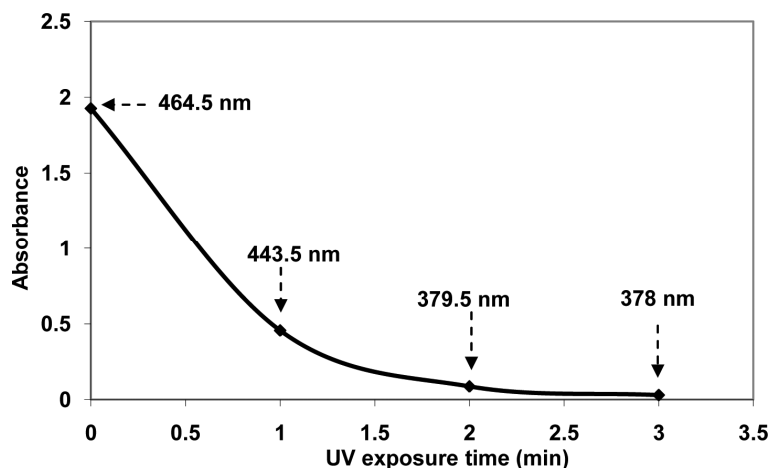
The initial absorption band without UV exposure is around $\lambda = 465$ nm. As the exposure time to UV increases, a shift of the absorption band towards the blue is observed and stabilises within 3 min around 378.5 nm in the UV region. As observed from the graph, the absorbance value of absorption peaks decreases rapidly towards zero within 3 min followed by the discolouration which reflects the complete disappearance of the MO. The

MO solution containing TiO_2 and H_2O_2 without exposure to UV radiations does not show any discolouration during one hour which suggests that UV radiations are the main actor in the loss of solution colour and degradation of the sample. The presence of H2O2 contributes to the amount of $HO^\bullet$ radicals (Zhong et al., 2008; Haque and Muneer, 2007). The chemical reaction mechanisms might be expressed by equations (10), (11), and (12).

The degradation of MO using UV radiations does not show any end product as already observed when exposed to the humid air plasma species. The presence of TiO_2 and H_2O_2 in the solution accelerates even further the degradation process. The major difference is that UV radiations involve electrons produced by TiO_2 (equations (8) and (9) while H_2O_2 directly liberates hydroxyl radicals (equation (10)). Plasma treatment introduces in the solution $^\bullet NO$ reactive species that react with degraded or cleaved MO to give a final product that could not be degraded.

3.2   pH measurements

The pH variation of MO, MO + TiO_2 and MO + H_2O_2 solutions was followed with the same period of treatment with humid air plasma and its behaviour is shown in Figure 10.

Figure 10 pH variation with treatment time for MO, MO + TiO_2 and MO + H_2O_2
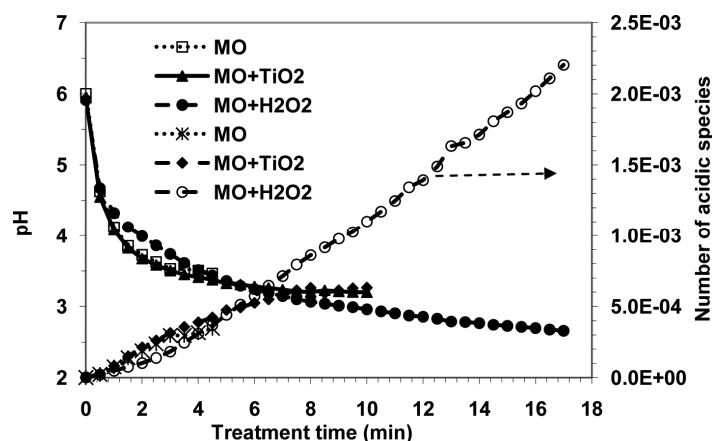
The initial solution with pH = 6 becomes more acidic with the treatment time as already observed in previous interactions with non thermal plasma with solutions (Benstaali et al., 1998; Janka and Maximov, 1997; Abdelmalek et al., 2004). The rapid increase of protons in the solution is due to the acidification process of plasma produced $^\bullet NO$ radicals and the simultaneous oxidation process of aromatic rings by $HO^\bullet$ radicals is favoured by highly acidic media (Benstaali et al., 1998). The rate of variation of the number of acidic species (protons + other acid ions) in the solution shows an interesting behaviour as shown in Table 3.

The rate of variation of the number of acidic species decreases from 10^{-4} in the range (464.5–495 nm) to nearly half (5×10^{-5}) in (495–415 nm) during the transformation of the dye. As we can see the time domain decreases as we go from MO to MO + TiO_2 to MO + H_2O_2. The rate of variation of pH in MO + H_2O_2 is half that of MO due maybe the fact that acid species produced such as NO_2 may be involved in interaction with the dye decreasing therefore the total number in the solution. It also could be due to the

recombination of plasma produced acid ions with hydrogen peroxide produced hydroxyl radicals in the solution. The loss in H bonds in the aromatic rings is the consequence of changes occurring in the absorption spectra and changes from one dye to another. The pH evolution with the exposure time to pH # 3.1 follows a classical titration plot of strong base by strong acid as already considered. It is worth being mentioned that the pK_as of Nitro-4-aniline and nitrous acid are 1.02 and 3.3 respectively. This suggests that nitrous acid/nitrite are the main products at the beginning of the plasma treatment and that nitro-4-aniline does not take a prominent place in pH control, which is consequent with the initial concentration of MO.

Table 3   Rate of variation of acidic species during plasma treatment during the different transformations of dyes

	464.5 – 495 nm	495 -415 nm	415 nm onwards
MO	10^{-4} (R^2=0.9921) [0 – 3 min]	5×10^{-5} (R^2=0.9759) [3.5 – 4.5 min]	
MO + TiO$_2$	10^{-4} (R^2=0.9888) [0 – 2.5 min]	6×10^{-5} (R^2=0.9924) [3.5 – 8]	
MO+H$_2$O$_2$	5×10^{-5} (R^2=0.9947) [0 – 1.5 min]	10^{-4} (R^2=0.9854) [2 – 4 min]	10^{-4} (R^2=0.9977) [4.5 - 17 min]

3.3 Electrolytic conductivity results

Electrolytic conductivity measurements have been performed in order to monitor chemical oxidation and acidification processes of MO and intermediate oxidation products, through the increase of solution conductivity due to the plasma production of highly reactive species. The electrolytic conductivity of the plasma treated MO + TiO$_2$ and MO + H$_2$O$_2$ has been measured and shown in Figure 11.

Figure 11 Conductivity variation of MO+TiO2 and MO+H2O2 vs. exposure time
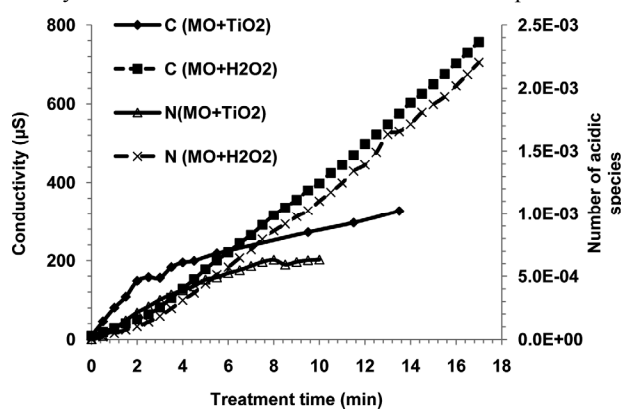
An initial electrolytic conductivity of 9.65 µS and 9.2 µS is obtained for MO + TiO$_2$ and MO + H$_2$O$_2$ respectively. A rapid increase of the conductivity is noticed in the time domain [0–2.5 min] for MO + TiO$_2$ while the rate of increase slightly decreases after 3 min treatment time. Plotting the number of acidic species in the solution against treatment time in the same graph shows a similar behaviour which suggests that the conductivity is directly related to species formed by the interaction of plasma with the solution. The rates of variation of the conductivity and the number of acidic species are given in Table 4.

Table 4   Rate of variation of conductivity and number of ionic species Solution

Solution	$d\sigma/dt$	dN/dt	$\sigma_{res}(\mu S/N)$
MO + TiO$_2$	67.86 (R^2=0.9977) [0 – 2 min]	10^{-4} (R^2=0.9803) [0 – 2 min]	6.09x10^{+5} (R^2=0.9751) [0 – 2 min]
	13.76 (R^2=0.9972) [3.5 – 15.5]	6x10^{-5} (R^2=0.9923) [3 – 8 min]	2.47x10^{+5} (R^2=0.9947) [2.5 – 8 min]
MO+H$_2$O$_2$	20.92 (R^2=0.9982) [0 – 2 min]	5x10^{-5} (R^2=0.9967) [0 – 2 min]	4. 08x10^{+5} (R^2=0.9992) [0 – 2 min]
	47.507 (R^2=0.9989) [2.5 – 17 min]	10^{-4} (R^2=0.9977) [2.5 – 17 min]	3.33 x10^{+5} (R^2=0.9991) [2.5 – 17min]

Recent study on electrochemical process as an alternative disinfection strategy for water purification showed that free chlorine is produced with smaller amounts of stronger oxidants, such as ozone, hydrogen peroxide and HO$^\bullet$ radicals and the increase in electrical conductivity was related to the increasing number of relatively small number HO$^\bullet$ radicals referred to as mixed oxidants (Jung et al., 2007). Acidic effect of plasma treatment is already attributed to $^\bullet$NO radicals. Previous experiment shows that diluted nitrous acid is expected in acidic media. Nitrogen (III) disproportionate to N(V) and N(II) and the concentration of NO$_2^-$ increase with the plasma treatment time before disappearing with a slightly lower rate. The last term of equation (4) is due to the degradation of the dye following the oxidation process. After the 2.5 min treatment time, the H bonds have completely oxidised resulting in another type of dye, therefore their contribution to the electrolytic conductivity decreases. The presence of other discharge products (HO$^\bullet$, H$_2$O$_2$, HO$_2$, NOx, ONOO$^-$) should be taken into account in the solution. It must be remembered that NO$_2^-$ and NO$_3^-$ ions are formed in an aqueous solution exposed to the gliding discharge. The concentration of formed nitrites presents a maximum as the exposure time increases, which indicates that NO$_2^-$ do not accumulate. Nitrites are actually destroyed because nitrous acid is thermodynamically unstable in acidic medium (pH < 2.6) and disproportionates to NO$_3^-$ and NO. Moreover, NO leads to NO$_2$ in contact with air, nitrogen dioxide reacts with OH in the presence of a third body to yield peroxynitric acid HOONO which iosomerises to nitric acid (Brisset at al., 2008).

Thus, the concentration of peroxynitrite must be taken into account for the conductivity balance, but it is unfortunately unknown.

The electrolytic conductivity is dependent on the contribution of different ionic species present in the solution, mainly, cations and anions derivatives of plasma produced reactive species $HO^{\bullet}$ and $^{\bullet}NO$ with the aqueous solution, we may write:

$$\sigma_s = \sigma_{ini} + n_+\sigma_+ + n\_\sigma\_ \tag{13}$$

where is the initial conductivity of the solution before treatment, n_+ σ_+ is the contribution of cations and $n\_\sigma\_$ is the contribution of anions to the conductivity.

3.4 Discussion

The variation of the absorption peak intensity of the initial MO with the exposure time to plasma results from the chemical oxidation processes the MO is undergoing under the interaction with the highly reactive species. The appearance of an intermediate orange-red dye at 495 nm is observed within the [0–2.5 min] treatment time with a shoulder at 525 nm. The appearance of the 495 nm absorption peak is dependent on the nature of catalyst added. In presence of H_2O_2, it appears earlier than for MO + TiO_2 and MO (Figure 12). Also the rate of DCO at 495 nm is steeper than the others (Figure 13).

Figure 12 Absorbance variation at 464.5 nm for MO, MO + TiO_2 and MO + H_2O_2
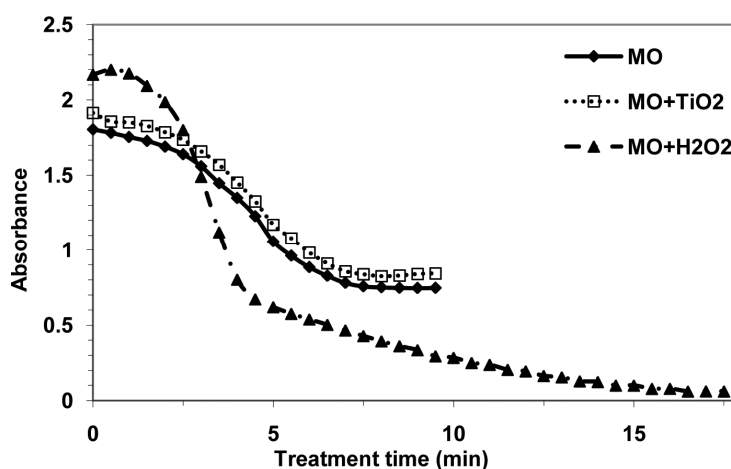
The presumably accelerated rate of chemical oxidation in MO + H_2O_2 is well illustrated in Figure 14 with the appearance of absorption peak 415 nm earlier (4 min) than MO and MO + TiO_2.

The progressive decrease follows just afterwards within 5 min giving rise to a final yellow product whose maximum peak of absorption is at 415 nm. As the pH of the solution decreases for longer treatment time, a diprotonated form $-^+NH-$ $(CH_3)_2$, $-N_\alpha = N_\beta H$ is expected to form at $\lambda = 410$ nm. The absorption peak of the final yellow product is observed at $\lambda = 415$ nm while it appears at $\lambda = 420$ nm in postdischarge plasma treatment (Brisset et al., 2008; Moussa et al., 2007). The final product is identified as the (N,N)-dimethyl-4nitro aniline obtained through oxidative cleavage of

the diazoic bond. The appearance of an isobestic point at 440 nm already observed in previous work is attributed to the exchange reaction taking place between the orange and the yellow forms of the dye. These two forms appear within the pH range [4.5–3]. As the shift of the absorbing wavelength from 464.5 to 495 nm occurs during the acidic evolution of the solution while the formation of an intermediate compound by reactions of the non-degraded MO molecules with fragments from degraded ones, other detection techniques like GC-MS or LC-MS might be useful in order to identify the reaction products and the reaction mechanism.

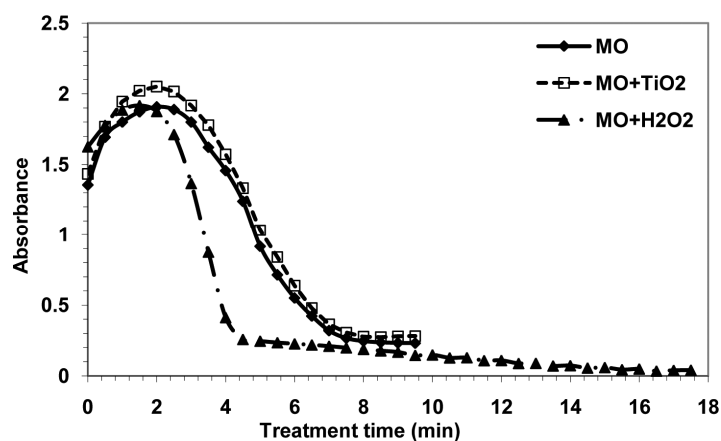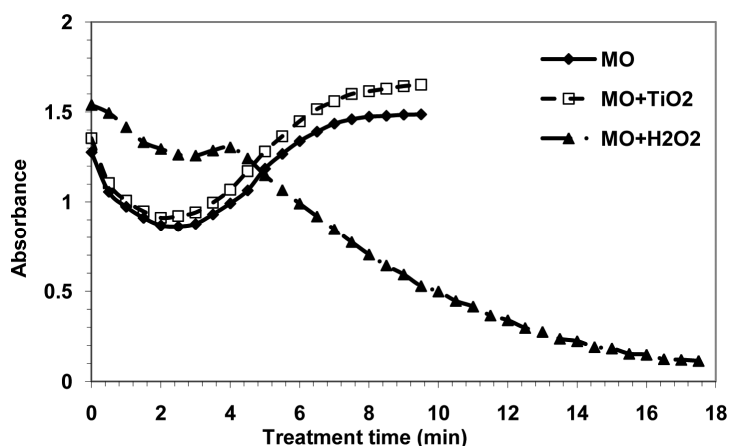**Figure 13** Absorbance variation at 495 nm for MO, MO + TiO$_2$ and MO + H$_2$O$_2$

Figure 14 Absorbance variation at 415 nm for MO, MO + TiO$_2$ and MO + H$_2$O$_2$

The changes in the rate of variation of the electrolytic conductivity of MO + TiO$_2$ and MO solutions may be attributed to the appearance of different conducting species involved in each solution. Exposing MO + TiO$_2$ + H$_2$O$_2$ to UV radiations leads to the discolouration of the dye which suggests that the only absent species are $^\bullet$NO radicals and their derivatives. Therefore the final product of plasma treated solutions contains nitrites that are difficult to degrade with plasmas.

Orange 3 behaves differently from Orange 1 and Orange 2 and does not present any azo-hydrazone tautomerism. But in acid medium, an ammonium-azonium equilibrium occurs in Orange 3 solution (Thomas and Burgess, 2007). When the azonium form becomes preponderant the solution is red. This form is already observed in strong acid medium (pH = 2.0) with an absorption peak at $\lambda = 506$ nm with a molecular absorption coefficient $\varepsilon = 39.180$ mol^{-1} L cm^{-1}. As the pH of the treated orange solution is over 3.0, the absorption peak of this form is shifted towards the red and appears at 525 nm.

4 Conclusion

The first objective in using atmospheric non thermal plasma for the treatment of MO was to degrade the dye. That objective was not completely reached since the final product after 15 min treatment time was still yellow and was not degraded. It was identified as N,N-dimethylnitro-4 aniline which results from the cleavage of the parent molecule MO. However exposing MO solutions with catalysts (TiO$_2$ and H$_2$O$_2$) to the highly reactive plasma produced species helps understand some of the chemical oxidation-acidification mechanisms that occur in the dye solution. H2O2 accelerates the reactions better than TiO$_2$. Methyl Orange undergoes direct chemical reactions in presence of plasma produced species that lead to transformations and structural changes resulting in a final product. This end product involves $^{\bullet}$NO radicals that are present in gliding arc discharges and totally inexistent in UV photocatalytic radiations. Further investigation is underway to understand the efficiency of the degradation of MO molecules involving more than one catalyst (TiO$_2$ and H$_2$O$_2$) and different sources: the plasma and UV radiations source.

Acknowledgement

References

Abdelmalek, F., Gharbi, S., Benstaali, B., Addou, A. and Brisset, J-L. (2004) 'Plasmachemical degradation of azo dyes by humid air plasma: Yellow Supranol 4GL, Scarlet Red Nylosan F3GL and industrial waste', *Water Res.*, Vol. 38, pp.2339–2347.

Benstaali, B., Boubert, P., Cheron, B.G., Addou, A. and Brisset, J.L. (2002) 'Density and rotational temperature measurements of OH$^{\bullet}$ and NO$^{\bullet}$ radicals produced by a gliding arc in humid air', *Plasma Chem. Plasma Proc.*, Vol. 22, No. 4, pp.553–571.

Benstaali, B., Boubert, P., Cheron, B.G., Addou, A. and Brisset, J.L. (1999) 'Spectral investigation of humid air plasma: a key to chemical application', *Proc. 14th Int. Sym. Plasma Chem.*, Praga, Czech Rep., Vol. II, pp.939–945.

Benstaali, B., Moussa, D., Addou, A. and Brisset, J.L. (1998) 'Plasma treatment of aqueous solutes: some chemical properties of a gliding arc in humid air', *Europ. Phys. J. Appl. Phys.*, Vol. 4, pp.171–179.

Brisset, J.L., Moussa, D., Doubla, A., Hnatiuc, E., Hnatiuc, B., Kamgang-Youbi, G., Herry, J.M., Naitali, M. and Bellon-Fontaine, M.N. (2008) 'Chemical reactivity of discharges and temporal post-discharges in plasma treatment in aqueous media: examples of gliding discharge treated solutions', *Ind. Eng. Chem. Res.*, Vol. 47, pp.5761–5781.

Darwent, J.R. and Lepre, A. (1986) 'Photo-oxidation of methyl orange sensitized by zinc oxide. Part 1', *Mechanism, J. Chem. Soc., Faraday Trans.*, Vol. 2, No. 82, pp.1457–1468.

Fillon, G., Czernichowski, A. and Lesueur, H. (1990) *Fr. Pat. 90- 11278.*

Gao, J. (2006) 'A novel technique for wastewater treatment by contact glow-discharge electrolysis', *Pakistan Journal of Biological Sciences*, Vol. 9, No. 2, pp.323–329.

Gong, J. and Cai, W. (2007) 'Degradation of methyl orange in water by contact glow discharge electrolysis', *Plasma Sci. Technol.*, Vol. 9, No. 2, pp.190–193.

Gong, J., Wang, J., Xie, W. and Cai, W. (2008) 'Enhanced degradation of aqueous methyl orange by contact glow discharge electrolysis using Fe_2^+ as catalyst', *J. Appl. Electrochem.*, Vol. 38, pp.1749–1755.

Grabowski, L.R., van Veldhuizen, E.M., Pemen, A.J.M. and Rutgers, W.R. (2007) 'Breakdown of methylene blue and methyl orange by pulsed corona discharge', *Plasma Sources Sci. Technol.*, Vol. 16, pp.226–232.

Guetta, N. and Ait Amar, H. (2005) 'Photocatalytic oxidation of methyl orange in presence of titanium dioxide in aqueous suspension. Part I: Parametric study', *Desal. Water Technol.*, Vol. 185, pp.427–437.

Haque, M.M. and Muneer, M. (2007) 'TiO_2-mediated photocatalytic degradation of a textile dye derivative, bromothymol blue, in aqueous suspensions', *Dyes and Pigments*, Vol. 75, No. 2, pp.443–448.

Hardin, I.R., Zhao, X. and Akin, D.E. (2003) 'Biotreatment approach to decolorizing textile waste effluents', in Kathryn, J.H. (Ed.): *Proc. 2003 Georgia Water Resources Conference*, pp.810–813.

Heba, A., Ashraf, A., Anwer, E. and Ibrahim, I. (2008) 'Treatment of textile waste water using H_2O_2/UV system', *Physiochemical Problems of Mineral Processing*, Vol. 42, pp.17–28.

Janka, J. and Maximov, A.I. (1997) 'Stimulation of the oxidation processes in the liquid solutions by means of gliding arc', *Proc. ICPIG –22*, Toulouse, France, T.1, pp.256–178.

Jorgensen, P., Chapelle, J., Czernichowski, A. and Meguernes, K. (1987) *Fr. Pat. 2 620 436.*

Jung, Y.J., Oh, B.S., Kang, J.W., Page, M.A., Phillips, M.J. and Marinas, B.J. (2007) 'Control of disinfection and halogenated disinfection byproducts by the electrochemical process', *Water Sci. Technol.*, Vol. 55, pp.213–219.

Lacheb, H., Puzenat, E., Houas, A., Ksibi, M., Elaloui, E., Guillard, C. and Hermann, J.M. (2002) 'Photocatalytic degradation of various types of dyes (Alizarin S, Grocein Orange G, Methyl Red, Congo Red, Methylene Blue) in water by UV-irradiated titania', *Appl. Catal. B: Environ.*, Vol. 39, pp.75–90.

Lesueur, H., Czernichowski, A. and Chapelle, J. (1988) *Fr. Pat. 2 639 172.*

Li, C., Tang, Y., Kang, B., Wang, B., Zhou, F., Ma, Q., Xiao, J., Wang, D. and Liang, J. (2007) 'Photocatalytic degrating methyl orange in water phase by UV-irradiated CdS carried by carbon nanotubes', *Sci. China Ser E-Tech. Sci.*, Vol. 50, No 3, pp.279–289.

Magureanu, M., Mandache, N.B. and Parvulescu, V.I. (2007) 'Degradation of organic dyes in water by electrical discharges', *Plasma Chem. Plasma Process*, Vol. 27, pp.589–598.

McCallum, J.E.B., Madison, S.A., Alkan, S., Depinto, R.U.R. and Wahl, R.U.R. (2000) 'Analytical studies on the oxidative degradation of the reactive textile dye Uniblue A', *Environ. Sci. Technol.*, Vol. 34, No. 24. pp.5157–5164.

Moussa, D., Doubla, A., Kamgang-Youbi, G. and Brisset, J.L. (2007) 'Postdischarge long life reactive intermediates involved in the plasma chemical degradation of an Azoic dye', *IEEE Transactions on Plasma Science*, Vol. 35, No.2, pp.444–453.

Mozia, S., Tomaszewska, M. and Morawski, A.W. (2005) 'Photocatalytic degradation of azo-dye Acid Red 18', *Desalination*, Vol. 185, pp.449–456.

Oakes, J. and Gratton, P. (1998) 'Kinetic investigations of the oxidation of Methyl Orange and substituted arylazonaphthol dyes by peracids in aqueous solution', *J. Chem. Soc., Perkin Trans.*, Vol. 2, pp.2563–2568.

Rashed, M.N. and El-Amin, A.A. (2007) 'Photocatalytic degradation of methyl orange in aqueous TiO_2 under different solar irradiation sources', *Int. J. Phys. Sci.*, Vol. 2, No. 3, pp.073–081.

Sengupta, S.K., Singh, R. and Srivastava, A.K. (1998) 'A study on non-faradaic yields of anodic contact glow discharge electrolysis using cerous ion as the OH scavenger: an estimate of the primary yield of OH radicals', *Indian J. Chem., Sect. A*, Vol. 37, No. 6, pp.558–560.

Sigma–Aldrich, IR-Spectra (3), 1450:D

Tasaki, T., Wada, T., Fujimoto, K., Kai, S., Ohe, K., Oshima, T., Baba, Y. and Kukizaki, M. (2009) 'Degradation of methyl orange using short-wavelength UV irradiation with oxygen micro-bubbles', *J. Hazard. Mater.*, Vol. 162, pp.1103–1110.

Telke, A., Kalyani, D., Jadhav, J. and Govindwar, S. (2008) 'Kinetics and mechanism of reactive Red 14. Degradation by a bacterial isolate rhizobium radiobacter MTCC 8161', *Acta Chim. Slov.*, Vol. 55, pp.320–329.

Thomas, O. and Burgess, C. (2007) *UV-visible Spectrophotometry of Water and Wastewater*, 1st ed., Elsevier, Amsterdam, p.50.

Yu, X.D., Qu, X.S., Guo, Y.H. and Hu, C.W. (2005) 'Photocatalytic dye methyl orange decomposition on ternary sulfide ($CdIn_2S_4$) under visible light', *Chinese Chem. Lett.*, Vol. 16, No. 9, pp.1259–1262.

Zhong, J., Ma, D., Zhao, H., Lian, A., Li, M.J., Huang, S. and Li, J. (2008) 'Photocatalytic decolorization of methyl orange solution with potassium peroxydisulfate', *Cent. Eur. J. Chem.*, Vol. 6, No. 2, pp.245–225.